Fast Terahertz Spectroscopic Holographic Assessment of Optical Properties of Diabetic Blood Plasma

Maksim S. Kulya[1] · Evgeniy L. Odlyanitskiy[1] · Quentin Cassar[2] ·
Ilia A. Mustafin[3] · Valery N. Trukhin[3] · Polina G. Gavrilova[1] ·
Dmitry V. Korolev[4] · Yulia A. Kononova[4] · Nikolay S. Balbekin[1] ·
Patrick Mounaix[2] · Jean-Paul Guillet[2] · Nikolay V. Petrov[1] ·
Olga A. Smolyanskaya[1]

Abstract

A new method for diagnosis of diabetes mellitus is proposed, which uses for measurement a lyophilized blood plasma sample prepared in the form of a pellet. The paper develops a methodology for fast spectroscopic measurements of such pellets with terahertz pulse time-domain holography. For that reason, blood plasma pellets were experimentally measured by terahertz time-domain spectroscopy system in transmission mode and its characteristics were obtained to be then used in numerical simulation of pulse terahertz hologram formation and extraction of its optical properties. Thus, a demonstration of the proof-of-concept was given for the techniques of pellet inspection, which contains information about the presence of glycated proteins, reflecting a diabetic pathology.

✉ Olga A. Smolyanskaya
   smolyanskaya@corp.ifmo.ru

1   Institute of Photonics and Optical Information Technologies, ITMO University,
    3 Kadetskaya str., 199004, Saint-Petersburg, Russia

2   IMS Laboratory UMR CNRS 5218, Bordeaux University, 351 Cours de la Liberation,
    33045, Talence, France

3   Ioffe Institute, 26 Politekhnicheskaya str., 194021, Saint-Petersburg, Russia

4   Almazov National Medical Research Centre, 2 Akkuratova str., 197341, Saint-Petersburg, Russia

1 Introduction

Modern terahertz (THz) systems for the diagnosis of biological objects are mainly based on the principles of THz pulse time-domain spectroscopy (TDS) and raster-scanning focal-plane imaging (RSFPI). The widespread use of these systems is due to their coherent detection approach that allows providing both the real and the imaginary parts of index of refraction [1]. Previous works reported the use of THz radiation at both the sub-cellular level and the super-cellular one. At the sub-cellular level, various candidates for interaction were reported to be sensitive to THz radiation such as biological water [2, 3], nucleic acids [4], proteins [5], lipids [6], and carbohydrates [7]. Sensing life sub-units is not an end on itself. The purpose behind these investigations is to understand the interaction mechanisms at a more complex stage, where sub-units gather to build tissues and organic fluids. Tissues and fluids are the sub-units of organs and thus are of primary importance when dealing with injuries, diseases, and disorders. Research towards biomedicine applications of THz waves at a super-cellular level can be separated into two axis: (i) in vivo diagnosis near the body surface and (ii) in vitro tissues and fluids. While the first axis mainly gathers skin [8, 9], eyes [10, 11], and teeth [12] examinations, the second one largely focuses on studies for oncology [13–16] and diabetes [17–19].

While for cancer, specific THz-sensitive markers are yet to be fully understood, THz waves were found to be sensitive to glycated protein concentration increase in blood plasma, which is often related to diabetes [20]. Changes among blood plasma composition caused by pathological processes may considerably affect its optical properties. Fasting glucose concentration in plasma collected from patients without glucose metabolism disorders lies in the range 3.3–6.1 mmol/L, while in diabetes mellitus glucose level is $\geq$ 7.0 mmol/L [21]. Increased glucose concentration leads to glycolization of proteins (albumin), which is a nonenzymatic process in which glucose attaches to the amino groups of proteins [22, 23]. Prior investigations on different soft tissues on both human and animals in vitro show that the optical properties of diabetic tissues differ from the ones of healthy tissues [24, 25]. However, studying soft tissues remains difficult to carry out since tissues dry out during the experiment and their biochemical and optical properties are progressively being modified. Investigations on whole blood are on their side tedious since blood cells (leukocytes, platelets, and red blood cells) are expected to be predominant in the THz frequency range [26], hence blurring glycated proteins' response. Therefore, one way to proceed is to study blood plasma as performed in [26]. Nevertheless, liquid samples are difficult to study since they cannot be stored for a long time and their biochemical properties are expected to change during the experiment. Suitable forms to study blood plasma properties are therefore lyophilized blood plasma prepared in the form of pellets [27]. Such samples are transportable and convenient to store. Moreover, they practically do not absorb moisture, they have low absorption in the THz frequency range, and they can be conveniently fixed in a vertical holder for THz TDS in transmission mode.

This work solves two important problems: (i) development of the THz diagnostic approach by popularizing the biological object's inspection in the form of specially prepared pellets. To do this, we finalized and described the methodology for preparing pellets of diabetes mellitus from two types of biological tissue: pathological

(diabetic) and healthy, and also studied their optical properties. The pellets are the tablets pressed from small-fractional protein crystals. Each crystal of pellets contains a certain percentage of fats (triglycerides), proteins (albumin), and fibrinogen—all of them normal or glycated (in diabetic case). This causes spatial inhomogeneities of the index of refraction of pellets. To obtain statistically reliable data about the pellets it makes sense to adapt the THz imaging, which provides two-dimensional surface inspection. Basically, THz-RSFPI coupled with TDS is able to deal with that, but its drawback is the long time it takes for a raster scanning. And this circumstance leads us to the formulation of the problem (ii): an adaptation for these measurements is the THz pulse time-domain holography (THz PTDH) as a tool providing the fast measurement during a single delay line passage. Previously, this technique has already demonstrated its ability to reconstruct a stepped and smooth relief of the technological objects that are sufficiently transparent in the THz frequency range [28, 29], and the prospects of application for biological objects were also considered [24, 30]. However, a complete related methodology has not been presented, and the specifics of its application in the tasks of inspection of such biological objects have not yet been described. An advantage of this technique is the ability to register in one pass the data delay line in three dimensions: two spatial and one temporal [31, 32]; and this is achieved by detecting the THz field onto a wide-aperture electro-optical crystal coupled to a matrix photodetector.

Figure 1 shows a conceptual diagram of objects (shown as red-framed elements) and actions (orange-framed elements). The diagram illustrates the main stages of given basic research (green arrows path), aimed at developing a methodology for the holographic assessment of blood plasma pellets, as well as the expected sequences of the actions that may be used directly in clinical practice (blue arrows path). The basic research, whose results are reported in this paper, contains two stages, namely physical and numerical experiments. The physical study, shown at the top sequence row of Fig. 1, involves pellet preparation (described in this work in Section 2.1) and characterization of their properties using THz-TDS (Section 2.2), while the numerical study (remaining two sequence rows on Fig. 1) deals with the development of THz PTDH approach laying the foundation for subsequent preparation of an experimental protocol for reliable express-diagnosis based on a single measurement. It includes a full cycle of solving direct and inverse diffraction problems.

The spatial distribution of the optical characteristics extracted by the TDS-RSFPI and information about object topology are used as initial data. In the case considered in the framework of this study, only the information on the pellet thickness should be known as topological characteristics. Using experimental data, the numerical model of the wavefield transmitted through the object is synthesized (Section 3.2). Then, using the THz PTDH mathematical approach, the raw THz hologram is simulated (as described in Section 3.3), and the setup response (it includes noise and features of the detection) is incorporated to such a hologram. Thus, a solution of the direct diffraction problem is obtained. Starting from this step (bottom sequence row of Fig. 1), the data emulates the results of real holographic measurements that can be obtained while using the technique during clinical practice. Here, the influence of the features of the detection process should be eliminated and the inverse diffraction problem is solved (Section 3.4). The noise reduction filters can be embedded in the processing
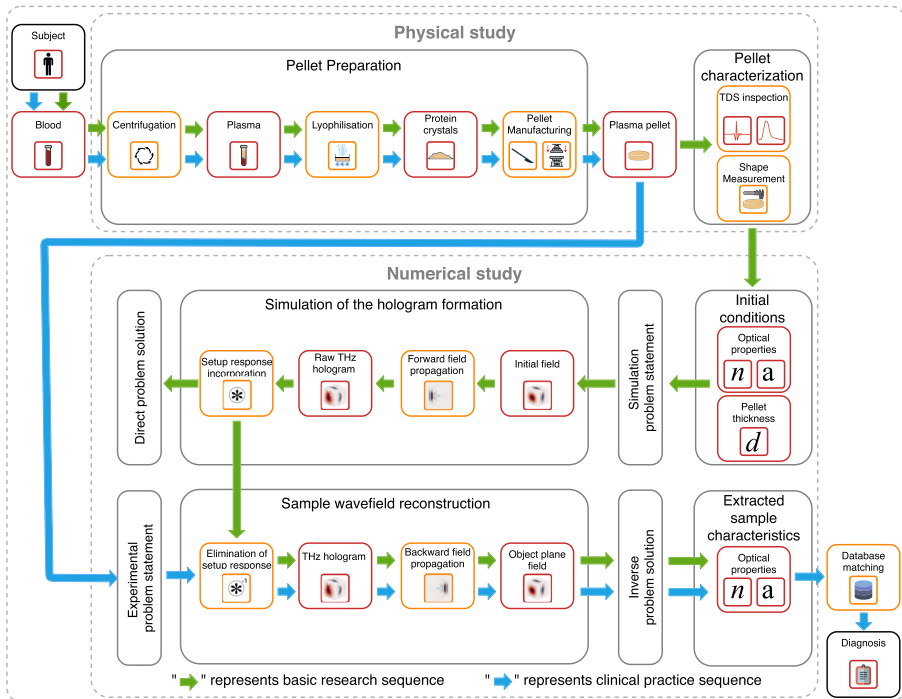
Fig. 1 Conceptual diagram of the THz PTDH method shows the current state of development and the possibilities of the THz holography method of diabetes express-diagnostics

algorithm responsible for numerical calculation of backward diffraction propagation of THz field and to the object plane [29, 33]. The obtained spatial-temporal profiles are then analyzed, and the possibility of calculating the optical characteristics of pellets based on holographic measurements is checked from the corresponding spatial distribution of a complex-valued time spectrum. In clinical practice, prepared pellets will be directly measured in an expanded collimated THz beam (the configuration of the experimental setup is discussed in Section 3.1). The spatio-temporal THz field waveforms diffracted on the pellet—THz holograms—will be measured, from which numerical models of the THz field in the object plane will be obtained. Then, the spatial distribution of optical properties of pellets will be extracted and statistically processed with further database matching for diagnosis.

2 Experimental Study of Optical Properties of Blood Plasma Pellets by THz TDS

2.1 Pellet Preparation

The study was carried out with samples of venous blood plasma taken from a male patient suffering from decompensated second type of diabetes mellitus and from a

healthy male participant, being 43 and 39 years old, respectively (Almazov National Medical Research Centre, Saint-Petersburg, Russia). All experimental protocols used in this investigation were reviewed and approved by the participants and the Local Ethics Committee. Venous whole blood was collected in the morning in an empty stomach after 8–12 h of fasting in a test tube with K_3EDTA. Blood plasma was obtained by centrifuging the blood during 15 min at a speed of 3000 revolutions per minute. Blood plasma samples were frozen at a temperature of -80 °C and lyophilized by freeze-drying $VaCo_2$ (ZirBus, Germany) at a temperature of -50 °C and a pressure of 3 Pa. Dried blood plasma represents a sponge composed of crystals. The sponge was destroyed by a metal spatula and crushed to a crystal size of several tens of micrometers. The use of a mortar and pestle was not possible due to the presence of various proteins in the plasma and grinding of proteins would lead to their unwanted adhesion and the formation of round granules. For dosing the samples into the matrix, a volumetric measure of 5 mm in diameter and 5 mm in height was used. The dry mixture of 200 mg blood plasma crystals has been pressed into a flat pellet in a steel press-mold with a diameter of 5 mm on a Corvette 590 hand press (Enkor, Russia) at a pressure of 500 kg/cm^2. The diameter of each pellet was 5 mm while measured thickness was 1.81 mm, "diabetic pellet," and 1.79, "non-diabetic pellet." The thickness of the pellets was fixed between two thin plates with a known thickness and measured using a mechanical micrometer with an accuracy of ± 10 μm. Pellets consist of biological crystals with average size of about tens of micrometers; some surface roughness of the pellets remains. The blood plasma pellets were a little fragile; therefore, this method for measuring the thickness prevented possible damages. We prepared ten diabetic and ten non-diabetic pellets. In a separate protocol, we draw up the averaged optical properties of these pellets in the THz frequency range. The dispersion of the heterogeneity of the index of refraction within the non-diabetic and diabetic pellets was around $\pm 9.9\%$ and $\pm 7.2\%$, respectively. In this work, we present an image of the restored optical properties of one non-diabetic and one diabetic pellet. Photographs of these pellets are presented below in Fig. 2. Visual characteristics of blood plasma pellets, illustrated in Fig. 2, are not reliable. Different physiological reasons may influence their color in visible EM range, for example, hemolysis (the release of blood cell content into plasma) or lipid concentration. Increased triglyceride concentration may cause turbidity, which also can be visible [34]. In clinical practice, diagnostic studies are carried out in liquid blood plasma using standardized methods and THz holographic reconstruction of optical properties in lyophilized plasma samples can be used as an additional tool for measuring the plasma properties.

2.2 Experimental Setup of THz Time-Domain Spectroscopy

THz-TDS has been around for over 30 years and has found widespread applicability with studies ranging from the study of electronic and transport properties of complex semiconductor nanostructures to biological and biomedical studies, such as cell detection (including blood, cancer, and bacterial cells). THz-TDS is a unique spectroscopic technique that allows determining the properties of a sample probed by short pulses of terahertz radiation [35].
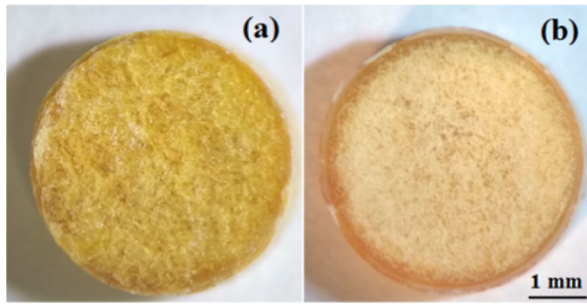
Fig. 2 Photographs of non-diabetic **a** and diabetic **b** pellets

To obtain experimental data that are necessary for calculating the index of refraction and the absorption coefficient of the pellets in the THz frequency range, a THz-TDS system was used (Fig. 3). This technique is based on coherent generation and detection of THz radiation. A Ti:sapphire laser reaches a beam splitter that splits the laser beam in half—pump pulse and probe pulse. The pump pulse passes through the delay line and excites an INAS epilayer grown on a semi-insulator GAAS wafer. Off-axis parabolic mirrors were used to form a paraxial THz beam, which comes at the optically nonlinear zinc telluride crystal. Concomitantly, the probe pulse focuses at the same point on the crystal. Displacement of the delay line allows to detain a probe pulse relatively to the THz pulse, which makes it possible to obtain a waveform of the THz pulse. Due to the interaction of the THz-wavefield with the probe light beam, the polarization of the probe beam changes in an electro-optical crystal, (EOC). This process is detected using the optical circuit that includes a quarter-wave plate λ/4, the Wollaston prism, WP, and the balance photo-detector, BPD (for more details see
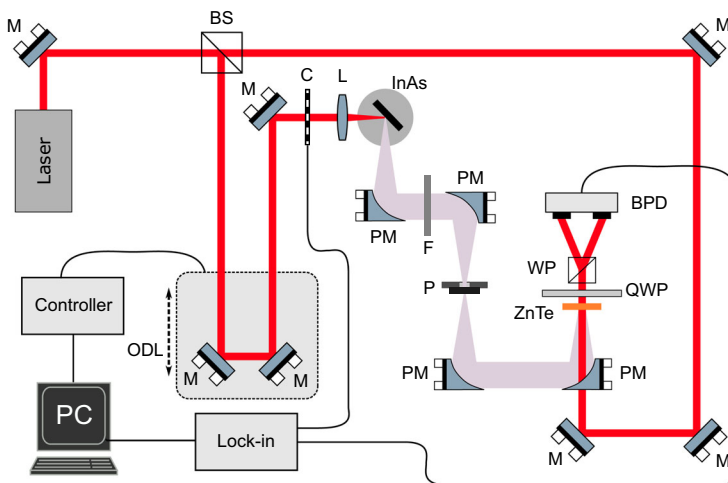

Fig. 3 Experimental setup of THz time-domain spectrometer

[27]). The pellets (P) were placed on the holder, which moves by means of motorized stages in the vertical and horizontal direction relative to the plane of incidence of the paraxial THz beam. In the usual case, the THz pulse was focused on the center of the pellet; however, in the case of the study of the uniformity of transmission, nine different points with corresponding coordinates (x, y) were studied.

During the experiment, waveforms, which are representing the dependence of the THz signal amplitude on the time delay between the pump pulse and the probe pulse, were recorded. These waveforms were obtained for THz pulses passing through the samples and through free space (without P on Fig. 3). To obtain the spectral components of the terahertz field, the fast Fourier transform (FFT) [36] was used. Based on part on the FFT results (spectral amplitude and phase), the index of refraction and absorption coefficient were derived.

2.3 Blood Plasma Pellet Optical Property Extraction

To calculate the optical properties of the objects (blood plasma pellets), the frequency dependence of amplitude $A(\omega)$ and phase $\varphi(\omega)$ was used. As a result, the following dependencies were calculated: $A_{ref}(\omega)$, $\varphi_{ref}(\omega)$, $A_{obj}(\omega)$, $\varphi_{obj}(\omega)$ [37].

Since the phase spectral dependencies had different values at zero frequency, a correction was carried out by means of linear approximation and phase shift.

Calculations were based on the equations for electromagnetic radiation passing through absorbing medium in the form of a plate with a thickness d [38]. For the ratio of complex amplitudes of the THz field of the pulse passing through the object and the free space, the following ratio can be obtained:

$$\frac{E_{ex}^s}{E_{ex}^r} = \frac{4 \cdot \tilde{n}}{(\tilde{n}+1)^2} \cdot \frac{1}{\left(1 - \frac{(\tilde{n}-1)^2}{(\tilde{n}+1)^2} e^{i2kd}\right)^2} \cdot e^{ik\tilde{n}d - \frac{\omega}{c}d}, \tag{1}$$

where $k = \frac{\omega}{c}$ is the wave vector, $\tilde{n} = n + i\kappa$ is the complex index of refraction, $\omega = 2\pi\nu$ is the angular frequency, and d is the object thickness.

Since we have chosen a time interval where only the first pulse is located and there are no THz pulses associated with the reflection of the THz wave from the object surfaces, the Eq. 1 can be simplified:

$$\frac{E_{ex}^s}{E_{ex}^r} = \frac{A_{ex}^s}{A_{ex}^r} \cdot e^{\varphi^s - \varphi^{ref}} = \frac{4 \cdot \tilde{n}}{(\tilde{n}+1)^2} \cdot e^{ik\tilde{n}d - \frac{\omega}{c}d}, \tag{2}$$

where $A_{ex}^s = |E_{ex}^s|$, $A_{ex}^r = |E_{ex}^r|$—.

Equation 2 indicates that there are no analytical expressions for n and κ from $\frac{A_{ex}^s}{A_{ex}^r}$ and $e^{\varphi^s - \varphi^{ref}}$. For the environments with absorption coefficient $\alpha < 100$ cm^{-1}, $\frac{n}{\kappa} \sim 0.03$ ($\nu \sim 1$ THz), which allows to count in the first approximation in the Eq. 2. Then, for spectral amplitudes and phases, respectively, we obtain:

$$\frac{A_{ex}^s}{A_{ex}^r} = \frac{4 \cdot n}{(n+1)^2} \cdot e^{-\frac{\omega}{c}\kappa d}, \tag{3}$$

$$\varphi^s - \varphi^{ref} = \frac{\omega}{c}nd - \frac{\omega}{c}d. \tag{4}$$

From Eq. 4, we obtain the index of refraction:

$$\frac{(\varphi^s - \varphi^{ref}) \cdot 0.3}{360 \cdot d \cdot v} + 1 = n. \tag{5}$$

If the index of refraction is known, and taking into account that $\frac{\omega}{c}\kappa = \frac{\alpha}{2}$, it becomes possible to calculate the absorption coefficient of the object from Eq. 3:

$$\alpha = \frac{2}{d} \ln \left(\frac{4 \cdot n \cdot E^{ref}}{(n+1)^2 \cdot E^s} \right). \tag{6}$$

3 THz PTDH Theory For Blood Plasma Pellet Study

3.1 THz PTDH Experimental Setup

The principle of THz PTDH operation is the same as THz-TDS, but the experimental setup has some differences. To eliminate the raster scanning requirement, we use broad collimated THz and IR beams for investigation of the necessary area of the object (Fig. 4). After passing a polarizer Gl$_1$, the probe beam is reflected by a BS to propagate collinearly to the EOC. The phase of the reflected from the EOC probe beam is modulated by the THz electrical field inside the EOC via Pockels effect, and this phase change is converted into intensity modulation by an analyzer Gl$_2$. A CMOS camera is used to catch the spatial distribution of the probe beam. The difference between two images with THz field on and off gives the THz distribution [39–41]. Also, the lens system can be used to match the diameter of the collimated IR beam with the CMOS matrix size. Such a scheme provides express registration of two-dimensional distribution of THz wavefield, which is important for the statistics collection.

3.2 Object Wavefront Simulation

We present here the mathematical model of THz hologram formation. Firstly, the initial real valued function of input THz pulse in temporal domain can be
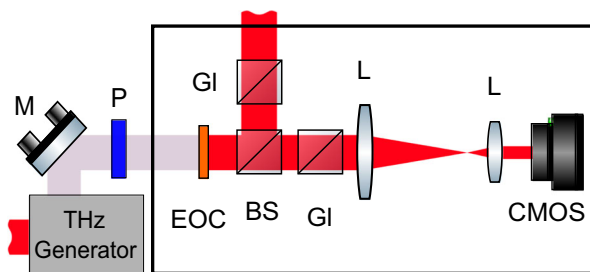

Fig. 4 Fragment of the THz PTDH experimental setup scheme

represented by the equation, describing the single-cycle electric field amplitude $E_{THz}(t)$ [42, 43]:

$$E_{THz}(t) = E_0 \frac{t}{\tau} \exp\left(-\frac{t^2}{\tau^2}\right), \tag{7}$$

where $t \in [-\frac{\tilde{t}_0}{2}; \frac{\tilde{t}_0}{2}]$, and $\tilde{t}_0$ is the time window size; E_0 is the amplitude of electric field in time-domain, and τ is the pulse duration. Then, electric field is decomposed by the Fourier integral to the complex spectrum form:

$$G_{THz}(\nu) = \int_{-\infty}^{\infty} E_{THz}(t) \exp(-i2\pi\nu t)\, dt. \tag{8}$$

To obtain THz wavefront after the investigated object (in our case, the blood plasma pellet), the initial complex spectrum $G_{THz}(\nu)$ is frequency-wise multiplied on the object function $O(x, y, \nu)$. Under "frequency-wise," we mean that object function is multiplied by initial spectrum for each frequency. In the calculation program, it is realized using "for loop" for all frequencies. This object function $O(x, y, \nu)$ contains both amplitude transmittance $T(x, y, \nu)$ and phase delay caused by refraction in the object $\varphi_{obj}(x, y, \nu)$. Knowing the information about the thickness $d(x, y)$, dispersion of the index of refraction $n_{obj}(x, y, \nu)$, and assuming the index of refraction of media around the object $n_{ref}(x, y, \nu) = 1$ (e.g., for the air), we can formalize the wavefront at the exit of the object plane:

$$\begin{aligned} G(x, y, \nu, z=0) &= G_{THz}(\nu) \cdot O(x, y, \nu) = G_{THz}(\nu) \cdot T(x, y, \nu) \exp(i\varphi(x, y, \nu)) \\ &= G_{THz}(\nu) \cdot T(x, y, \nu) \exp\left(i\frac{2\pi\nu}{c}\left(n_{obj}(x, y, \nu) - 1\right) d(x, y)\right), \end{aligned} \tag{9}$$

where c is the speed of light in vacuum. Note, that here we assume the thin object approximation where the diffraction inside the object is neglected. We also formalize the coordinate, corresponding to the object position, i.e., the exit of the object plane, to be $z = 0$ mm.

3.3 THz Hologram Formation

Formation of the pulsed THz hologram occurs when input wavefront after the object $O(x, y, \nu)$ propagates some distance in the media until registration plane. To perform the propagation of the initial wavefront to the arbitrary plane z, we use the spectral approach theoretically described in [44, 45]. In these papers, the applicability of the spectral equations for broadband single-cycle THz beam nonparaxial propagation is demonstrated. This spectral approach is based on two-dimensional complex wavefield decomposition to the angular spectrum:

$$C(f_x, f_y, \nu, z=0) = \int_{-\infty}^{\infty}\int_{-\infty}^{\infty} G(x, y, \nu, z=0) \exp\left(-2\pi i\left(x f_x + y f_y\right)\right) dx\, dy. \tag{10}$$

Then, the equations for the transverse g_x and longitudinal g_z spectral component's propagation in homogeneous isotropic dielectric media with an arbitrary complex index of refraction are formalized:

$$
\begin{cases}
g_x\left(f_x, f_y, \nu, z\right) = C\left(f_x, f_y, \nu, z_o\right) \exp\left(i\frac{2\pi \nu n(\nu)}{c}\Xi \cdot z\right) \\
g_z\left(f_x, f_y, \nu, z\right) = \frac{2\pi f_x \cdot C\left(f_x, f_y, \nu, z_o\right)}{\frac{2\pi \nu n(\nu)}{c}\Xi} \exp\left(i\frac{2\pi \nu n(\nu)}{c}\Xi \cdot z\right),
\end{cases}
\tag{11}
$$

where taking into consideration the condition for the radicand

$$
\Xi = \begin{cases}
\sqrt{1 - \frac{c^2}{\nu^2 n^2(\nu)}\left(f_x^2 + f_y^2\right)}, \; if \; \left(f_x^2 + f_y^2\right) \le \frac{\nu^2 n^2(\nu)}{c^2}; \\
i\sqrt{1 - \frac{c^2}{\nu^2 n^2(\nu)}\left(f_x^2 + f_y^2\right)}, \; if \; \left(f_x^2 + f_y^2\right) > \frac{\nu^2 n^2(\nu)}{c^2}.
\end{cases}
\tag{12}
$$

Note, that the second condition with imaginary root corresponds to the evanescent waves, which describes the loss of the energy during wavefront propagation.

Furthermore, reverting back from the spatial frequencies (f_x, f_y) to the original spatial coordinates (x, y) by the inverse 2D Fourier integral, we obtain the spectrum of the field propagated over the distance z:

$$
G\left(x, y, \nu, z\right) = \int_{-\infty}^{\infty}\int_{-\infty}^{\infty} g\left(f_x, f_y, \nu, z\right) \exp\left(2\pi i\left(x f_x + y f_y\right)\right) df_x df_y.
\tag{13}
$$

Then, 1D inverse Fourier transform for the propagated spectrum $G\left(x, y, \nu, z\right)$ allows reconstructing the temporal form of the field $E\left(x, y, t, z\right)$:

$$
E\left(x, y, t, z\right) = \int_{-\infty}^{\infty} G\left(x, y, \nu, z\right) \exp\left(i2\pi \nu t\right) d\nu.
\tag{14}
$$

Thus, we consider the registered electric field $E(x, y, t, z)$ as a pulsed THz hologram.

The setup resonance, which includes the features of the detection process and the noise generation model, must be taken into account in order to simulate the THz hologram view closer to the real one. In this paper, we consider quite a simple setup response model for the wavefield detection on a wide-aperture EOC. The response features of THz PTDH setups with a detection system based on a raster-scanning diaphragm were considered earlier in [29, 33, 46].

3.4 Object Optical Property Reconstruction

Reconstruction of the object properties is connected with inverse problem of wavefront propagation. For this purpose, complex spectrum $G(x, y, \nu, z)$ in registration plane z is numerically back-propagated to the initial object plane $z = 0$ by the previously described method. Such reconstructed wavefront allows us to study the spectroscopic properties of the object [24, 28, 30, 31], accounting a spatial distribution of complex index of refraction dispersion of the object's material [47].

To estimate the object properties $O(x, y, \nu)$ in Eq. 9, we need to divide the spectrum amplitude $G(x, y, \nu, z = 0)$ by the initial THz spectrum $G_{\text{THz}}(x, y, \nu)$. Thus, amplitude transmittance $T(x, y, \nu)$ in each (x, y) point is represented as:

$$T(x, y, \nu) = \left| \frac{G(x, y, \nu, z = 0)}{G_{\text{THz}}(x, y, \nu)} \right|, \tag{15}$$

and phase properties of the investigated object will be presented as phase difference between the input and reconstructed wavefronts:

$$\varphi(x, y, \nu) = \arg\left(G(x, y, \nu, z = 0)\right) - \arg\left(G_{\text{THz}}(x, y, \nu)\right). \tag{16}$$

Thus, the spatial distribution of index of refraction could be extracted from Eq. 9 if knowing the information about the object thickness $d(x, y)$ in each point:

$$n_{obj}(x, y, \nu) = 1 + \frac{\varphi(x, y, \nu) \cdot c}{2\pi\nu \cdot d(x, y)}. \tag{17}$$

4 Numerical Simulation of Phase Imaging of Pellets

We have designed the numerical model of blood plasma pellet with the following parameters: object thickness was 1.81 mm (diabetic pellet) and 1.79 (non-diabetic pellet); the field of view at the object and detection planes was 5×5 mm^2 with the pixel dimensions of 128×128 pixels; distance between object and detector was 5 mm. THz pulse duration τ was 0.65 ps with the corresponding spectrum interval approximately from 0.2 to 1.2 THz. The number of points N in the temporal profile was 1024; the time window size $\tilde{t}_0$ was equal to 95 ps. The phase according to Eq. 9 is simulated by plane mask with thickness $d(x, y)$. The spatial distribution of index of refraction $n(x, y, \nu)$ constructed from experimentally measured data (see Section 2.3) and resized to 128×128 pixels.

Due to the direct measurement of the electric field by THz PTDH, we have the initial data of $E(x, y, t, z)$. Thus, we can plot spatio-temporal distribution of the field in the object plane. These results are presented in Fig. 5 for non-diabetic and diabetic pellets. This picture represents the spatio-temporal slice of 3D data $E(x, y, t)$. Here, we fix y coordinated at the center ($y = y_0$) and plot $E(x, t)$.

Time delay in the field of diabetic case is caused by the local difference in the index of refraction of the pellet. This time delay could be observed also in THz-TDS, but only point-by-point for the focused beam. The huge advantage of THz PTDH is that we can register the wide-aperture collimated wavefront simultaneously using CMOS camera, and thus getting spatio-temporal structure of the investigated field, as presented below.

Analyzing the data in spectral domain $G(x, y, \nu, z)$, we can visualize amplitude and phase distribution and compare the information for individual frequency component. Figure 6 demonstrates amplitude and phase spatial distribution. For amplitude pictures corresponding to the diabetic case, we can observe some diffraction caused by local absorption in the pellet.

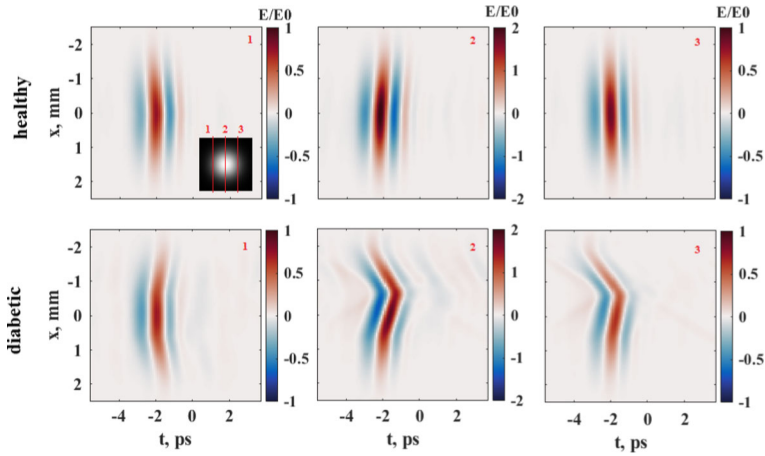Phase images also demonstrate some phase differences between non-diabetic and diabetic pellets

Fig. 5 Time domain image for non-diabetic and diabetic pellets for different cross sections of the THz beam. Cross-section regions are depicted by red lines 1, 2, 3 in the inset of the first image. This inset illustrates transverse profile of the beam which corresponds to Gaussian intensity distribution

More valuable information than phase images is reconstructed index of refraction of the pellets, which can be obtained using Eq. 17 . Figure 7 depicts this reconstructed index of refraction for different frequencies for non-diabetic and diabetic pellets. The spatial distribution of n for non-diabetic pellet preserves its homogeneity for different frequencies. Contrary to this, the distribution the index of refraction for diabetic pellet has several local inhomogeneities. These local inhomogeneities are presented in the inset of Fig. 7 by blue dotted circles. This is a clear illustration on how THz PTDH allows distinguishing spatially distributed spectroscopic information.
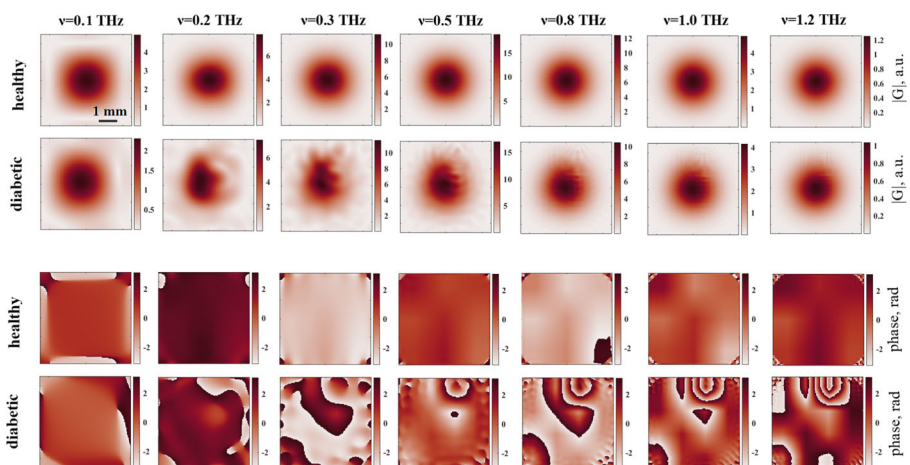

Fig. 6 Spatial distribution of spectral amplitude (2 upper rows) and phase (2 lower rows) for non-diabetic and diabetic pellets
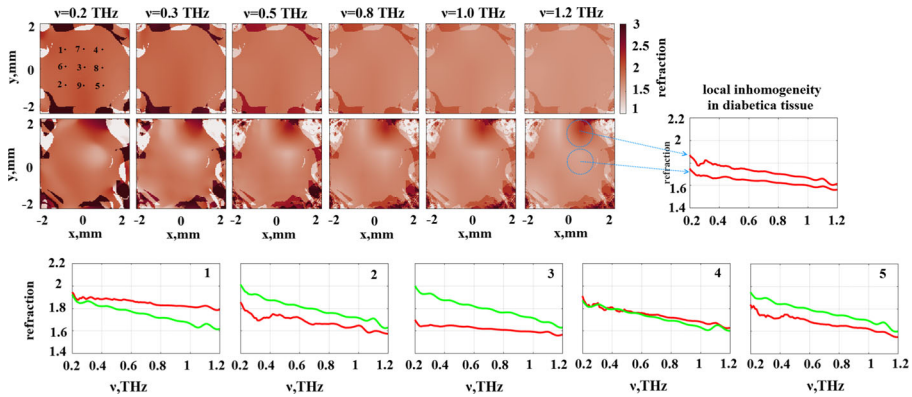
Fig. 7 Spatial distribution of reconstructed index of refraction for non-diabetic and diabetic pellets. Labels 1–5 show spatial points where we plotted index of refraction versus frequency. Green line corresponds to non-diabetic pellet and red corresponds to the diabetic one

At point 4 of Fig. 7, the optical properties of the blood plasma pellets (diabetic and non-diabetic) do not show significant differences. This may be due to the fact that non-diabetic and diabetic pellets may contain glycated and non-glycated proteins in different concentrations. Thus, at a given point, glycation of proteins could be similar in diabetic and non-diabetic pellets; therefore, their optical properties are similar. Analyzing the frequency-dependent character of index of refraction, we also plotted $n(\nu)$ for fixed spatial positions (labels 1–5), both for non-diabetic and diabetic pellets. In these specific points (except 4th), we can observe the sufficient differences in index of refraction in range 0.2–1.2 THz.

From a biological point of view, patients with decompensated diabetes mellitus are characterized by a change in many parameters (increased concentration of glucose, lipids, glycated proteins). Increased triglyceride concentration, which is common for diabetic patients, may cause turbidity of plasma [34]. Both diabetic and non-diabetic plasma pellets could contain glycated and non-glycated proteins in different concentrations. These factors could lead to inhomogeneity of pellets.

The results of proposed holographic approach correlates well with the results of RSFPI technique described in the work [48]. While THz-RSFPI was applied for non-destructive visualization of an inhomogeneous structure in the coated theophylline pellets, we focused our holographic approach on the inspection of blood plasma pellets. Both techniques are capable of providing images of acceptable quality, but the advantage of the holographic approach is the rapid imaging in a single pass of the delay line.

In this subsection, we demonstrated the ability of the holographic approach to reconstruct spatial properties of the investigated objects in terms of 2D distribution of the index of refraction, as well as frequency-dependent refraction in each point of the sample. Note that we shown the applicability of the THz PTDH method to the specific case of biological objects where the magnitude of absorption is relatively low and where the index of refraction has local features to be resolved.

5 Conclusion

A new approach for diagnosis of diabetes mellitus is proposed, which uses THz measurement of a lyophilized blood plasma sample prepared in the form of pellets. Since pellets are the pressed tablets from small-fractional crystals from triglycerides, albumin, and fibrinogen, their surface contains certain roughness and their internal composition is characterized by spatial inhomogeneities of the index of refraction. At the same time, they were relatively uniform and quasi-flat to effectively transmit THz radiation, and can be used in holographic measurements to obtain a spatially resolved distribution of optical properties providing statistically reliable results.

In our experiments, we created and characterized pellets from the venous blood plasma of healthy and suffering from the decompensated second type of diabetes mellitus male patients. Using information obtained by TDS-RSFPI about optical properties of the pellets, we synthesized a numerical model of the corresponding spatio-temporal distribution of THz broadband wavefield and assessed the capabilities of pulse time-domain holography for obtaining authentic information required for a diagnosis of diabetic disease. Thus, we have laid the foundations of a new approach for the diagnostics of human diabetes using innovative THz equipment and special proteins contained in the blood as a marker. This approach is being tested now at the Almazov Medical Center (St. Petersburg, Russia), and in the nearest future we expect the appearance of novel express-diagnostics tools based on it.

References

1. M. R. Grootendorst, A. J. Fitzgerald, S. G. B. De Koning, A. Santaolalla, A. Portieri, M. Van Hemelrijck, M. R. Young, J. Owen, M. Cariati, M. Pepper *et al.*, Use of a handheld terahertz pulsed imaging device to differentiate benign and malignant breast tissue, Biomed. Opt. Express **8**, 2932–2945 (2017).
2. J. Kindt and C. Schmuttenmaer, Far-infrared dielectric properties of polar liquids probed by femtosecond terahertz pulse spectroscopy, J. Phys. Chem. **100**, 10373–10379 (1996).
3. U. Møller, D. G. Cooke, K. Tanaka, and P. U. Jepsen, Terahertz reflection spectroscopy of Debye relaxation in polar liquids, J. Opt. Soc. Am. B **26**, A113–A125 (2009).
4. T. H. Duong and K. Zakrzewska, Calculation and analysis of low frequency normal modes for DNA, J. Comput. Chem. **18**, 796–811 (1997).
5. A. Markelz, A. Roitberg, and E. J. Heilweil, Pulsed terahertz spectroscopy of DNA, bovine serum albumin and collagen between 0.1 and 2.0 THz, Chem. Phys. Lett. **320**, 42–48 (2000).
6. M. Hishida and K. Tanaka, Long-range hydration effect of lipid membrane studied by terahertz time-domain spectroscopy, Phys. Rev. Lett. **106**, 158102 (2011).
7. H.-B. Liu and X.-C. Zhang, Dehydration kinetics of D-glucose monohydrate studied using THz time-domain spectroscopy, Chem. Physics Lett. **429**, 229–233 (2006).
8. M. H. Arbab, D. P. Winebrenner, T. C. Dickey, A. Chen, M. B. Klein, and P. D. Mourad, Terahertz spectroscopy for the assessment of burn injuries in vivo, J. Biomed. Opt. **18**, 077004 (2013).

9. I. Echchgadda, J. A. Grundt, M. Tarango, B. L. Ibey, T. D. Tongue, M. Liang, H. Xin, and G. J. Wilmink, Using a portable terahertz spectrometer to measure the optical properties of in vivo human skin, J. Biomed. Opt. **18**, 120503 (2013).

10. D. B. Bennett, Z. D. Taylor, P. Tewari, R. S. Singh, M. O. Culjat, W. S. Grundfest, D. J. Sassoon, R. D. Johnson, J.-P. Hubschman, and E. Brown, Terahertz sensing in corneal tissues, J. Biomed. Opt. **16**, 057003 (2011).

11. D. B. Bennett, Z. D. Taylor, P. Tewari, S. Sung, A. Maccabi, R. S. Singh, M. O. Culjat, W. S. Grundfest, J.-P. Hubschman, and E. R. Brown, Assessment of corneal hydration sensing in the terahertz band: in vivo results at 100 GHz, J. Biomed. Opt. **17**, 097008 (2012).

12. N. Hoshi, Y. Nikawa, K. Kawai, and S. Ebisu, Application of microwaves and millimeter waves for the characterization of teeth for dental diagnosis and treatment, IEEE T. Microw. Theory. **46**, 834–838 (1998).

13. C. B. Reid, A. Fitzgerald, G. Reese, R. Goldin, P. Tekkis, P. O'Kelly, E. Pickwell-MacPherson, A. P. Gibson, and V. P. Wallace, Terahertz pulsed imaging of freshly excised human colonic tissues, Phys. Med. Biol. **56**, 4333 (2011).

14. C. B. Reid, G. Reese, A. P. Gibson, and V. P. Wallace, Terahertz time-domain spectroscopy of human blood, IEEE J. Biomed. Health **17**, 774–778 (2013).

15. Q. Cassar, A. Al-Ibadi, L. Mavarani, P. Hillger, J. Grzyb, G. MacGrogan, T. Zimmer, U. R. Pfeiffer, J.-P. Guillet, and P. Mounaix, Pilot study of freshly excised breast tissue response in the 300–600 GHz range, Biomed. Opt. Express **9**, 2930–2942 (2018).

16. U. R. Pfeiffer, P. Hillger, R. Jain, J. Grzyb, T. Bucher, Q. Cassar, G. MacGrogan, J.-P. Guillet, P. Mounaix, and T. Zimmer, Ex Vivo Breast Tumor Identification: Advances Toward a Silicon-Based Terahertz Near-Field Imaging Sensor, IEEE Microw. Mag. **20**, 32–46 (2019).

17. O. Cherkasova, M. Nazarov, and A. Shkurinov, Noninvasive blood glucose monitoring in the terahertz frequency range, Opt. Quant. Electron. **48**, 217 (2016).

18. O. Smolyanskaya, E. Lazareva, S. Nalegaev, N. Petrov, K. Zaytsev, P. Timoshina, D. Tuchina, Y. G. Toropova, O. Kornyushin, A. Y. Babenko *et al.*, Multimodal Optical Diagnostics of Glycated Biological Tissues, Biochemistry (Moscow) **84**, 124–143 (2019).

19. O. Smolyanskaya, N. Chernomyrdin, A. Konovko, K. Zaytsev, I. Ozheredov, O. Cherkasova, M. Nazarov, J.-P. Guillet, S. Kozlov, Y. V. Kistenev *et al.*, Terahertz biophotonics as a tool for studies of dielectric and spectral properties of biological tissues and liquids, Prog. Quant. Electron. (2018).

20. O. Cherkasova, M. Nazarov, A. Angeluts, and A. Shkurinov, Analysis of blood plasma at terahertz frequencies, Opt. Spectrosc. **120**, 50–57 (2016).

21. W. H. Organization *et al.*, Definition and diagnosis of diabetes mellitus and intermediate hyperglycaemia: report of a WHO/IDF consultation, (World Health Organization, 2006).

22. K. J. Welsh, M. S. Kirkman, and D. B. Sacks, Role of glycated proteins in the diagnosis and management of diabetes: research gaps and future directions, Diabetes Care **39**, 1299–1306 (2016).

23. J. Anguizola, R. Matsuda, O. S. Barnaby, K. Hoy, C. Wa, E. DeBolt, M. Koke, and D. S. Hage, Glycation of human serum albumin, Clin. Chim. Acta **425**, 64–76 (2013).

24. O. Smolyanskaya, I. Schelkanova, M. Kulya, E. Odlyanitskiy, I. Goryachev, A. Tcypkin, Y. V. Grachev, Y. G. Toropova, and V. Tuchin, Glycerol dehydration of native and diabetic animal tissues studied by THz-TDS and NMR methods, Biomed. Opt. Express **9**, 1198–1215 (2018).

25. S. Sakhnov, E. Leksutkina, O. Smolyanskaya, A. Usov, S. Parakhuda, Y. V. Grachev, and S. Kozlov, Application of femtotechnologies and terahertz spectroscopy methods in cataract diagnostics, Opt. Spectrosc. **111**, 257 (2011).

26. O. A. Smolyanskaya, O. V. Kravtsenyuk, A. V. Panchenko, E. L. Odlyanitskiy, J. Guillet, O. P. Cherkasova, and M. Khodzitsky, Study of blood plasma optical properties in mice grafted with Ehrlich carcinoma in the frequency range 0.1–1.0 THz, Quantum Electron. **47**, 1031 (2017).

27. O. A. Smolyanskaya, V. N. Trukhin, P. G. Gavrilova, E. L. Odlyanitskiy, A. V. Semenova, Q. Cassar, J.-P. Guillet, P. Mounaix, K. G. Gareev, and D. V. Korolev, Terahertz spectra of drug-laden magnetic nanoparticles, Proc. SPIE **10892**, 108920L (2019).

28. N. V. Petrov, M. S. Kulya, A. N. Tsypkin, V. G. Bespalov, and A. Gorodetsky, Application of terahertz pulse time-domain holography for phase imaging, IEEE T. THz. Sci. Techn. **6**, 464–472 (2016).

29. M. Kulya, N. V. Petrov, A. Tsypkin, K. Egiazarian, and V. Katkovnik, Hyperspectral data denoising for terahertz pulse time-domain holography, Opt. Express **27**, 18456–18476 (2019).

30. N. S. Balbekin, Q. Cassar, O. A. Smolyanskaya, M. S. Kulya, N. V. Petrov, G. MacGrogan, J.-P. Guillet, P. Mounaix, and V. V. Tuchin, Terahertz pulse time-domain holography method for phase imaging of breast tissue, Proc. SPIE **10887**, 108870G (2019).

31. N. S. Balbekin, M. S. Kulya, A. V. Belashov, A. Gorodetsky, and N. V. Petrov, Increasing the resolution of the reconstructed image in terahertz pulse time-domain holography, Sci. Rep. **9**, 180 (2019).

32. M. S. Kulya, N. S. Balbekin, A. A. Gorodetsky, S. A. Kozlov, and N. V. Petrov, Vectorial terahertz pulse time-domain holography for broadband optical wavefront sensing, Proc. SPIE **11279**, 112790D (2020).

33. M. Kulya, N. V. Petrov, V. Katkovnik, and K. Egiazarian, Terahertz pulse time-domain holography with balance detection: complex-domain sparse imaging, Appl. Optics **58**, G61–G70 (2019).

34. R. Sepetiene, R. Sidlauskiene, and V. Patamsyte, Plasma for Laboratory Diagnostics, in *Plasma Medicine-Concepts and Clinical Applications,* (IntechOpen, 2018).

35. K. Ahi, N. Jessurun, M.-P. Hosseini, and N. Asadizanjani, Survey of terahertz photonics and biophotonics, Optical Engineering **59**, 061629 (2020).

36. C. Rønne, P.-O. Åstrand, and S. R. Keiding, THz spectroscopy of liquid H_2O and D_2O, Phys. Rev. Lett. **82**, 2888 (1999).

37. A. G. Davies, A. D. Burnett, W. Fan, E. H. Linfield, and J. E. Cunningham, Terahertz spectroscopy of explosives and drugs, Mater. Today **11**, 18–26 (2008).

38. M. Born and E. Wolf, *Principles of optics: electromagnetic theory of propagation, interference and diffraction of light* (Elsevier, 2013).

39. Z. Jiang and X.-C. Zhang, 2D measurement and spatio-temporal coupling of few-cycle THz pulses, Optics Express **5**, 243–248 (1999).

40. Q. Wu, T. Hewitt, and X.-C. Zhang, Two-dimensional electro-optic imaging of thz beams, Applied Physics Letters **69**, 1026–1028 (1996).

41. Z. Lu, P. Campbell, and X.-C. Zhang, Free-space electro-optic sampling with a high-repetition-rate regenerative amplified laser, Applied Physics Letters **71**, 593–595 (1997).

42. A. Koulouklidis, V. Y. Fedorov, and S. Tzortzakis, Spectral bandwidth scaling laws and reconstruction of THz wave packets generated from two-color laser plasma filaments, Phys. Rev. A **93**, 033844 (2016).

43. Y. A. Kapoyko, A. A. Drozdov, S. A. Kozlov, and X.-C. Zhang, Evolution of few-cycle pulses in nonlinear dispersive media: Velocity of the center of mass and root-mean-square duration, Phys. Rev. A **94**, 033803 (2016).

44. A. Ezerskaya, D. Ivanov, V. Bespalov, and S. Kozlov, Diffraction of single-period terahertz electromagnetic waves, J. Opt. Technol. **78**, 551–557 (2011).

45. A. A. Ezerskaya, D. V. Ivanov, S. A. Kozlov, and Y. S. Kivshar, Spectral approach in the analysis of pulsed terahertz radiation, J. Infrared Millim. Te. **33**, 926–942 (2012).

46. M. Kulya, N. Petrov, A. Tcypkin, and V. Bespalov, Influence of raster scan parameters on the image quality for the thz phase imaging in collimated beam with a wide aperture, J. Phys. Conf. Ser. **536**, 012010 (2014).

47. M. Kulya, N. Balbekin, I. Gredyuhina, M. Uspenskaya, A. Nechiporenko, and N. Petrov, Computational terahertz imaging with dispersive objects, J. Mod. Optic. **64**, 1283–1288 (2017).

48. A. Novikova, D. Markl, J. A. Zeitler, T. Rades, and C. S. Leopold, A non-destructive method for quality control of the pellet distribution within a MUPS tablet by terahertz pulsed imaging, Eur. J. Pharm. Sci. **111**, 549–555 (2018).